Reduced Pin-Count Test Strategy for 3D Stacked ICs Using Simultaneous Bi-Directional Signaling Based Time Division Multiplexing

IFTIKHAR A. SOOMRO[ID], **MOHAMMAD SAMIE**[ID], **AND IAN K. JENNIONS**[ID]

School of Aerospace, Transport and Manufacturing, Cranfield University, Cranfield MK43 0AL, U.K.

Corresponding author: Iftikhar A. Soomro (i.soomro@cranfield.ac.uk)

ABSTRACT 3D Stacked Integrated Circuits (SICs) offer a promising way to cope with the technology scaling; however, the test access requirements are highly complicated due to increased transistor density and a limited number of test channels. Moreover, although the vertical interconnects in 3D SIC are capable of high-speed data transfer, the overall test speed is restricted by scan-chains that are not optimized for timing. Reduced Pin-Count Testing (RPCT) has been effectively used under these scenarios. In particular, Time Division Multiplexing (TDM) allows full utilization of interconnect bandwidth while providing low scan frequencies supported by the scan chains. However, these methods rely on Uni-Directional Signaling (UDS), in which a chip terminal (pin or a TSV) can either be used to transmit or receive data at a given time. This requires that at least two chip terminals are available at every die interface (Tester-Die or Die-Die) to form a single test channel. In this paper, we propose Simultaneous Bi-Directional Signaling (SBS), which allows a chip terminal to be used simultaneously to send and receive data, thus forming a test channel using one pin instead of two. We demonstrate how SBS can be used in conjunction with TDM to achieve reduced pin count testing while using only half the number of pins compared to conventional TDM based methods, consuming only 22.6% additional power. Alternatively, the advantage could be manifested as a test time reduction by utilizing all available test channels, allowing more parallelism and test time reduction down to half compared to UDS-based TDM. Experiments using 45nm technology suggest that the proposed method can operate at up to 1.2 GHz test clock for a stack of 3-dies, whereas for higher frequencies, a binary-weighted transmitter is proposed capable of up to 2.46 GHz test clock.

INDEX TERMS Reduced pin-count testing, 3D SICs, time division multiplexing, test access mechanism, simultaneous bidirectional signaling.

I. INTRODUCTION

The transistor density in 2D integrated circuits has been exponentially increasing following Moore's law over the past several decades; however, shrinking technology further is now proving difficult due to thermal and power constraints [1]. A promising way forward is to stack the individual dies vertically in the third dimension creating a single package known as 3D Stacked Integrated Circuit (SIC). 3D SICs overcome the problems of increasing interconnect path delays and offer higher performance with a much smaller footprint.

The associate editor coordinating the review of this manuscript and approving it for publication was Yong Chen[ID].

This concept has been applied successfully to manufacture processors, memories, and FPGAs [2]–[4].

One of the key enablers allowing 3D stacking of dies is the vertical interconnects between the dies, known as Through Silicon Vias (TSVs). However, TSVs bring about additional challenges for testing [5]. First, TSVs occupy a significant chip area, and therefore, there is a limit on the TSVs that could be included in the design, and even more so for testing purposes. The limited number of TSVs reduces the test channel width available for transportation of test vectors to and from the tester. Moreover, the increased number of dies means higher transistor count and an increased number of test patterns now need to be applied, and unlike 2D ICs, not just once but at several instances during stacking of the dies,

such as pre- mid- and post-bond testing. It is evident that as the test vector volume and the number of test instances increase, the test access bottleneck caused by TSVs becomes significant.

Nevertheless, TSVs allow very high bandwidth owing to smaller channel resistance [6]. However, the same cannot be utilized in testing as the scan chains restrict the maximum shift frequency. The Flip-Flops, in the design, are converted to scan-enabled flops after the functional front-end design to enable scan-based tests. Consequently, the Flip-Flops, now concatenated as shift registers forming a scan-chain, are not optimized for timing. Because of these timing constraints and the thermal and power constraints associated with higher switching activity during testing, the maximum shift frequency of the scan-chain is restricted to a few tens of MHz and results in under-utilization of channel bandwidth and increased test times. One solution is to send in the test data at a high frequency and incorporate a mechanism to distribute the data among multiple scan chains at a lower frequency, such as by using Serializer-Deserializer (SerDes) or Time Division Multiplexing (TDM). By utilizing the full channel bandwidth, fewer pins or TSVs would be required and is termed as Reduced Pin Count Testing (RPCT) [7]. RPCT also results in a reduced number of test equipment channels needed for testing a device, and the spare channels can be utilized to test multiple devices in parallel, also known as Multi-Site Testing [8], [9].

This paper proposes a TDM based RPCT technique coupled with simultaneous Bi-Directional Signaling (SBS). In contrast with the conventional TDM based technique, which uses a communication channel in a uni-directional fashion by either sending or receiving data at a particular time, SBS allows simultaneous transmission and reception of the data in a channel. The advantage of such a technique could be a reduction in the number of test channels required for a given Test Access Mechanism (TAM) or a decrease in test time for a given number of test channels.

The rest of the paper is organized as follows. In section II, the motivation for this work and the prior work in TAM design methods using RPCT techniques and SBS is presented. In section III, we introduce the principle of operation of TDM and SBS. SBS-TDM based test strategy for 3D SIC is presented in section IV. Evaluation results of the proposed SBS-based method versus UDS-based TDM test method are presented in section V, followed by the conclusion in section VI.

II. MOTIVATION AND PRIOR WORK

Testing is of vital importance as it ensures defect-free and reliable devices. However, with the ever-advancing transistor density, the test times and hence the cost of chips increase significantly [10], opening the focus of significant research in such areas. The most commonly used Design for Test (DfT) strategy is scan-based testing, which involves shifting-in the test stimuli vectors serially, applying the test stimuli, and scanning out of the response vectors. The test application points are the memory elements or the flip-flops in the design, which are modified such that these are observable and controllable in test mode and are termed as scan-flops. The scan-flops are then concatenated into serial shift-registers, known as scan chains, such that the test data could be sequentially scanned in and out using the core's primary inputs and outputs. The stimuli could be propagated through the intermediate combinational logic, and the response could be read out for comparison with the expected response. With millions of flip-flops expected in modern core-based design, a single serial scan mechanism such as an IEEE 1149.1 standard compliant JTAG port [11] may not be suitable in terms of test times. Parallel test ports, such as Wrapper Parallel Ports (WPP) of the IEEE 1500 Standard [12], allow the use of multiple serial scan channels by temporarily using the I/Os for test purposes. The test standard relying on similar serial/parallel test access mechanisms is also introduced for 3D-SICs [13].

Despite using the parallel test ports during testing, the exponentially increasing transistor density and the limited number of chip terminals do not allow all the scan-chains to be accessed at once. Therefore, the test process is segmented into sessions, and during each session, only a limited number of cores are accessed and tested. A number of test patterns are scanned in one bit at a time, making the entire process significantly time-consuming and costly. In general, the test time increases with the test data volume (and hence the chip complexity) and decreases with the available channel width for parallel test ports and the scan shift frequency. Test compression methods have been frequently employed to reduce the test data volume [14]. However, this method requires additional on-chip resources such as decompressors and compactors. Also, beyond a certain point, test compression reduces the test coverage. Increasing the available channel width for parallel test ports significantly reduces the test time [15], [16], but the bottleneck, in this case, is the limited number of chip terminals and TSVs in the design. Increasing the scan shift frequency offers a proportional reduction in test times; however, the most critical limiting factor, in this case, are the scan-chains that are not optimized for timing and operate on low frequency. This results in the loss of usable tester and the chip terminal/TSV bandwidth which are capable of much higher speeds.

RPCT based methods have two significant advantages. First, it allows optimal utilization of the tester and I/Os bandwidths, and secondly uses fewer chip terminals than Full Pin Count Testing. Additionally, in 3D-SICs, the wafers are thinned to expose the TSVs hidden in the substrate [5], [17], and the thinned die may not be able to withstand the forces exerted by the tester probes; and therefore, only limited test channels may be available. Hence, RPCT naturally lends itself to testing 3D-SICs. Techniques such as SerDes and TDM, which allow increasing the scan frequency while addressing the scan chains' low frequency, have been frequently employed to achieve RPCT.

A TDM based access mechanism for serial Reconfigurable Scan Networks (RSNs), such as those based on IEEE 1687 standard (aka iJTAG) [18], was proposed in [19]. Unlike traditional scan design, an RSN allows dynamic scan path reduction as and when required. However, using a single serial access interface limits the practicability of such an approach for high volume test vector transportation. The future SICs are expected to contain millions of flip-flops necessitating high bandwidth scan-testing employing Parallel Test Ports. The authors in [20] and [21] highlighted the notion of using virtual TAMs and Serializer and De-serializer (SerDes). In [22], the authors discuss a combination of test vector compression and RPCT to reduce test times. The authors in [23] proposed using Multi-Valued Logic (MVL) for tester-to-chip communication. The use of MVL increases the data rate for a given clock frequency; however, they necessitate analog to digital converter with calibration schemes which may complicate the implementation and add significant chip area.

Much of the above work has been focused on 2D chips, and a majority of these methods are applicable to 3D designs as well. Nonetheless, the implementation is not straightforward, and 3D technology-specific concerns must be considered. The Test Access Mechanism (TAM) design, which refers to the insertion of required logic between the chip's primary I/Os and the individual cores to enable test vector transport, is known to be an NP-Hard combinatorial problem. The design choice of a TAM such that the test requirements of all the dies in 3D SIC are met using limited resources significantly affects the test time. Several researchers focus on test time reduction by optimal TAM design for 3D SICs [24], [25]. The authors in [26], [27] proposed a TDM based RPCT test strategy in 3D-SICs. In [27], the authors showed significant improvement in test times using TDM compared to conventional TAM design methodology. The authors defined 'global channels' as communication channels traversing vertically through multiple TSVs/dies, as opposed to point-to-point communication channels (the same definition of 'global channels' will be used in this article). The global channels were operated at a higher frequency, and the data were multiplexed to dies, and in turn to the cores at lower frequencies.

The focus of the previous research work in testing and test time reduction has been on conventional UDS signaling. This simplifies the design as the standard I/O cells can be utilized; however, Simultaneous Bidirectional Signaling (SBS) significantly improves the throughput of communication channels, significantly impacting test time. The author in [28] briefly discussed the dynamics of using SBS in chip testing and its future potential. The research in SBS has been mostly focused on the normal mode (as opposed to test mode), point to point communication links, focusing on throughput and power efficiency. Following the initial concept of SBS by the authors in [29], the researchers have proposed various methods to enable SBS. Broadly, the SBS design methodology can be classified into differential [30], [31] or single-ended designs [29], [32]–[34], current mode [30], [31] or voltage mode

transceivers [33], [29], [34], or based on channel characteristics such as on-chip [30], [35] or off-chip communication [29], [32]. 3D SICs offer a promising prospect for SBS due to the low channel impedance of the TSVs. The authors in [36], [37] proposed single-ended SBS design methodologies for use in 3D SICs and reported significant improvement in chip area, throughput, and power consumption compared to 2 x UDS-based TSVs.

While both TDM/ SerDes and SBS methods improve the efficiency of a communication channel, the key difference is that the former is aimed at maximizing the use of available channel bandwidth, whereas the latter allows using a single pin to form the communication channel. The previous works have focused on using these methods separately in the chip testing scenario, with SBS used to decrease the test time [38], and TDM/ SerDes used to minimize test channels (pins/ TSVs) [27]. Nevertheless, a combination of both methods presents new prospects in the 3D SIC test, allowing minimization of test resources as well as test time reduction. This, however, presents several challenges. Firstly, the previous research in SBS has been focused on conventional point-to-point communication, which simplifies the implementation. In this scenario, communication is required between a high-frequency source at the near-end (Scan-in vectors from the tester) and several far-end transmitters operating at much slower speeds (Scan-out vectors from the scan chains), for which the design is not straightforward. Secondly, unlike [38], where SBS was used in the Full Pin Count Test (FPCT) scenario with the low-frequency operation, the design considerations in this case are complicated by high-performance requirement.

This paper explores the feasibility of integrating SBS with TDM based RPCT method, with a particular focus on its application in testing 3D SICs. We present a potential SBS transceiver design capable of high-frequency operation and evaluate the design tradeoffs. The design challenges and possible solution of integrating SBS with 2D-TDM based Test Access Mechanism, which requires a global channel traversing through multiple TSVs, are studied. Moreover, the strategy to extend TDM-SBS based test methodology to pre- mid- and post-bond test instances of 3D SICs is presented.

III. BACKGROUND

This section describes the operation of TDM based test methodology, followed by an overview of Simultaneous Bidirectional Signaling. The working concept is illustrated using example cases that mainly focus on scan-based test architectures. The same examples will be subsequently used as the test cases for evaluation.

A. TIME DIVISION MULTIPLEXING

Consider an example 3D-SIC with three dies, as shown in Fig. 1. It is assumed that every die is composed of 2 cores with a total of 3 scan chains and that all dies are identical (details are only shown for the first die for clarity). In general,
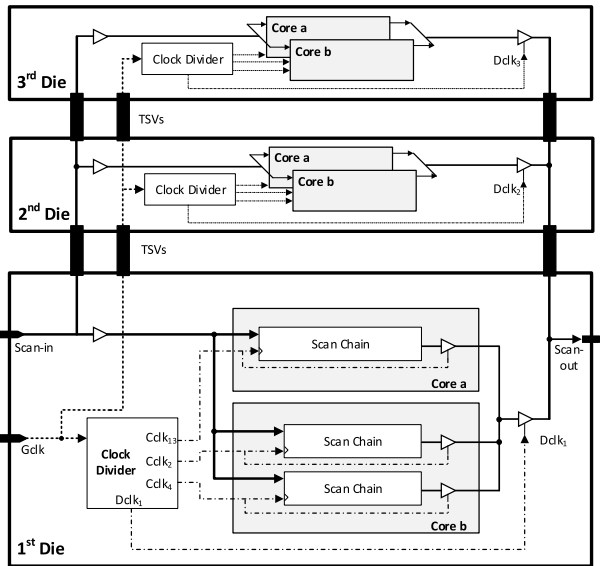
FIGURE 1. An example implementation of TDM for scan-test application based on [27].
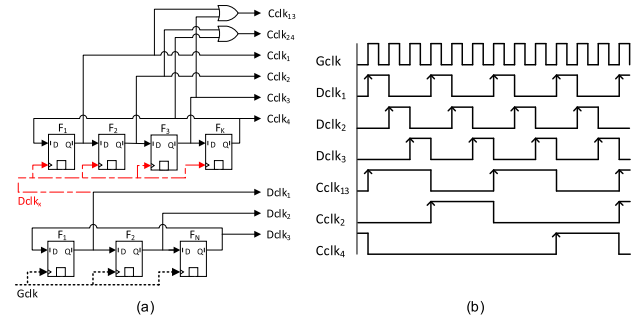

FIGURE 2. Control circuit for TDM (a) Generation of core and die clocks from global test clock using ring counters, the bottom RC generates die clocks, the top RC generates core clocks (b) timing diagram of the die and core clocks.

the number of scan chains is far greater than the available number of test channels and depending on the test schedule, only a small subset of cores are selected at a time. Therefore, this example represents the case for a particular test session in the overall test schedule. A single test channel is shown, which originates at the scan-in chip terminal and terminates at the bottom die's (1st die) scan-out chip terminal. It is assumed that the tester communicates with the 1st die through these chip terminals.

The TDM design for this example is based on the method proposed in [27] in which the authors proposed using separate 2D-TDM for the vertical (inter-die) and horizontal (intra-die) communication. At the input, the incoming data is available to all the dies, and in turn, the scan chains, using the global TSV channel. The data is demultiplexed from the Scan-in pin to the cores by controlling the scan chains' clock signal, such that data is scanned-in only to the scan chain which receives the positive clock edge. At the scan-chain output, the data is multiplexed on the scan-out pin using two tri-state buffer stages. The first stage tri-state buffers (one for every scan-chain) are controlled such that only one buffer is active at a time, essentially serving as 3 to 1 multiplexer. In the second stage, tri-state buffer (one for every die) in-turn multiplexes the data onto the scan-out pin, one die at a time.

To appropriately demultiplex the data at the input and multiplex at the output, the above arrangement requires a control circuit to select the appropriate die, core, and hence the scan-chain at every clock cycle. This is achieved using a clock divider circuit that can be constructed using shift registers as a Ring Counter (RC). Fig. 2 (a) shows one implementation of the clock divider circuit. The incoming Global Clock signal (*Gclk*) is first divided to generate Die clock (*Dclk*). As there are three dies in this example, a 3-bit RC is used to generate three 120° out of phase die clocks (Dclk$_{1,2,3}$) running at 1/3rd

of the *Gclk* frequency. To ensure this, the RC is initialized with a one-hot bit sequence (with only one bit set high - 100-bit sequence used in this case). The die clock serves two purposes; First, it allows multiplexing the data to the Scan-out pin by activating the second stage tri-state buffer of only one die at a time (Fig. 1). Secondly, it is used to derive the Core Clock (*Cclk*) signals for the individual cores/scan chains, as shown in Fig 2(a). The *Cclks* serve two other purposes, first, they allow demultiplexing the data from the scan-in terminal to the scan chains, and secondly, they activate the first stage tri-state buffer of the cores to be multiplexed at the output.

The choice of the number of flip-flops for *Cclk* generation would determine the lowest achievable frequency (*fmin*) and the number of scan chains serviceable by the *Cclk*. For *k* flip-flops, a minimum frequency of *Dclk/k* can be achieved, and at most, *k* scan-chain can be multiplexed. Multiples of *fmin* can also be produced by OR-gating alternate *Cclk* outputs, as shown in Fig. 2(a). In this way, different frequency clocks can be provided to scan-chains depending on the scan-frequency supported by the core. For example, in Fig 1, the *Cclk$_{13}$*, which is twice the minimum core clock frequency (*Dclk/k*), is used to serve the scan-chain chain in the *core a* of the dies. Fig 2 (b) shows the timing diagram of the derived clock signals. The clock division using this arrangement produces a duty cycle with on-time equal to the clock period of the *Gclk*, ensuring the second stage tristate buffers are 'on' for the entire *Gclk* cycle.

B. SIMULTANEOUS BI-DIRECTIONAL SIGNALING

Conventional TAM design using TDM requires separate output and an input port to form a test channel, as shown in Fig. 3(a). The proposed TAM design is based on Simultaneous Bi-Directional Signaling (SBS) in which a channel could be formed using one pin only, as illustrated in Fig. 3(b). SBS is different from traditional bi-directional pins in that the latter can only be configured either as an input or an output at a given time (half-duplex) and is therefore considered to be UDS for test purposes.

The working principle of SBS is elaborated using an example die consisting of a single scan chain of two-bit length,
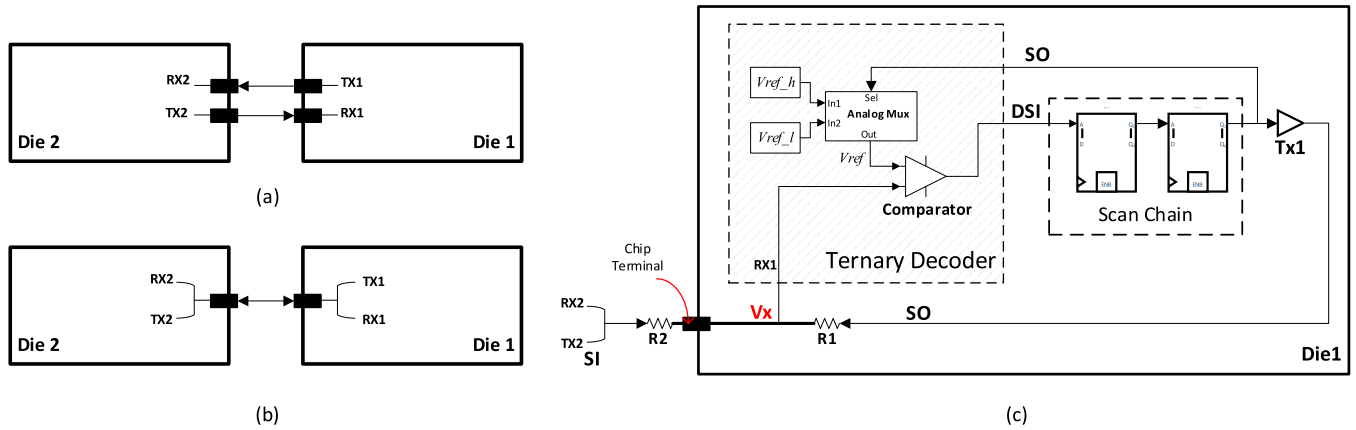
FIGURE 3. An illustration of simultaneous Bi-directional signaling (a) Conventional Uni-directional signaling using two wires (b) Simultaneous Bi-directional signaling using one wire (c) Block diagram of SBS working principle–test channel formation for a two-bit scan chain.

as illustrated in Fig. 3(c). Using a conventional UDS scheme, two pins would be required, one to connect the input of the scan-chain to the Scan-In (*SI*) signal and another pin to connect the output of the scan-chain Scan-Out (*SO*) (Fig. 3a). However, using SBS, a single pin could transmit and receive *SO* and *SI* simultaneously. To achieve the same, the signal at the chip terminal is ternary encoded instead of binary. The scan-chain SO's output is fed to a transmitter *Tx1*, which could be designed as a buffer. The *Tx1* (with an output impedance of *R1*) drives the chip terminal from one end, whereas a similar transmitter *Tx2* (with output impedance *R2*) is assumed to be driving the same chip terminal with the *SI* signal from another die (In Fig. 3(c) the *R1* and *R2* depict transmitter internal impedance but are shown as external resistors for clarity). Depending on the state of the *SI* and *SO*, the voltage *Vx* at the chip terminal node will either be pulled low (0 V) or high (Vdd) in the case when both ends are being driven low or high, respectively; however, *Vx* will take on an intermediate value (*Vxm*) when both transmitters are in the opposite state (10 or 01). The value of *Vxm* will depend on the impedances *R1* and *R2*, and assuming both to be the same, *Vxm* equates to 1/2 Vdd.

The ternary encoded signal *Vx* at the chip terminal can now be used by each die to determine whether the incoming signal (*SI*) is the same or opposite of the signal (*SO*) being trans-mitted. The Ternary Decoder (TD) block shown in Fig. 3(c) receives the *Vx* signal and the *SO* signal (taken just before *Tx1*). To determine the *Vx* signal state, two reference voltages are required, a high reference voltage *Vrefh* that is midway between Vdd and *Vxm*, and a low reference voltage *Vrefl* halfway between *Vxm* and the ground. An analog multiplexer is employed, selecting *Vrefh* if *SO* is high and *Vrefl* when *SO* is low. A voltage comparator circuit is used to compare the *Vx* signal with the *Vref* (reference voltage from the Analog Multiplexer). Table 1 lists all possible SI and SO values and the state of the transceiver in each case. When *SO* is 1, *Vx* can only take on the value of 1 (Vdd) or *Vxm* (1/2 *Vdd). A high value at *Vx* implies that *SI* must also be high, whereas a 1/2
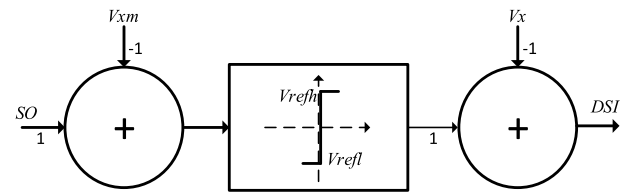

FIGURE 4. Neural network presentation of the ternary decoder.

*Vdd voltage level indicates *SI* must be zero. The comparator determines the same by comparing *Vx* with *Vref* from the Analog Multiplexer, which in this case (*SO* = 1) would be *Vrefh*. Similarly, When *SO* is low, the comparator receives the lower reference *Vrefl* and compares it with *Vx*, which could either be low (meaning *SI* = 0) or 1/2 *Vdd (meaning *SI* = 1). In all cases, the Decoded Scan-In (*DSI*) Signal produced by the comparator (and hence the TD) is the same as the original *SI*, as shown in Table 1.

A mathematical presentation of the ternary decoder can be constructed using a neural network shown in Fig. 4. The output DSI can be represented with (1), where *U* is the step function:

TABLE 1. SBS transceiver states.

SO	SI	Vx	Vref	Vx>Vref	DSI
0	0	0	Vrefl	False	0
0	1	½*Vdd	Vrefl	True	1
1	0	½*Vdd	Vrefh	False	0
1	1	1	Vrefh	True	1

$$DSI = U\left(V_x - \left[V_{refl}\,U\,(V_{xm} - SO) + V_{refh}\,U\,(SO - V_{xm})\right]\right) \quad (1)$$

V_{GND} and V_{dd} in Fig. 5 are constant values, while Vx varies depending on the *SO* and *SI* voltages. The position of Vx is determined by the superposition of *SO* and *SI* applied to the resistive network comprised from *R1* and *R2*, calculated
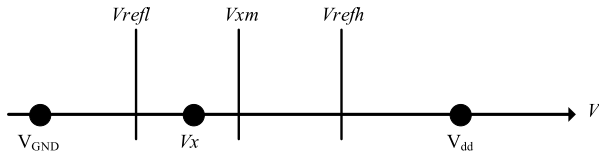
FIGURE 5. Hyperplanes created by the neurons in Fig. 4.

using the following equation:

$$V_x = SI \frac{R_2}{R_1 + R_2} + SO \frac{R_1}{R_1 + R_2} \tag{2}$$

The neurons in the network of Fig. 4 generate two hyperplanes, a fixed position hyperplane of *Vxm*, and a dynamic position hyperplane of *Vref*. This initially compares the input value *Vx* with the fixed hyperplane *Vxm*, then based on the result, it triggers *Vrefl* if *Vx* < *Vxm*, otherwise *Vrefh* if *Vx* > *Vxm*. Fig. 5 demonstrates a case when *Vrefl* is triggered as the valid hyperplane for the second neuron because of *Vx* < *Vxm*. Finally, in accordance with Table 1, the network generates logic value '1' as *Vx* > *Vrefl*.

IV. METHODOLOGY

This section demonstrates the feasibility of using SBS-based TDM using the test case of UDS-based TDM design presented in section III and modify it to include an SBS transceiver, as shown in Fig. 6. The design of an SBS transceiver is dependent on the characteristics of the channel; therefore, the design considerations are different for the communication channel between the tester and the first Die, and for inter-die communication (using TSVs). As the TSV channel is much less resistive in nature [6], the design for an SBS transceiver is relatively simple and can be achieved using the core transistors. Therefore, to avoid complexity, we assume that tester-to-die communication is done using the existing UDS method, and we only propose SBS for inter-die communication through TSVs.

A. TRANSCEIVER DESIGN

SBS transceivers can be implemented using several design methods. Differential mode transceivers [39] are used for high-frequency applications; however, the design is often complicated, and the requirement of two wires limits its use in TAM design where single-ended one wire systems are preferable. Single-ended SBS transceivers for use in the TDM scheme require three main components, the transmitter, receiver, and the control circuit, including TDM switching circuitry.

The transmitter design mostly depends on two factors, the required performance and the power consumption. As the SBS transmitter involves ternary coding, the design deviates from the static CMOS logic to generate the intermediate voltage levels, resulting in high static currents. The transmitter was designed as an inverter, followed by a Transmission Gate (TG) acting as an analog switch, as shown in Fig. 7 (a). The TG allows turning off the transmitter when not in use; for instance, to limit static current or during functional mode
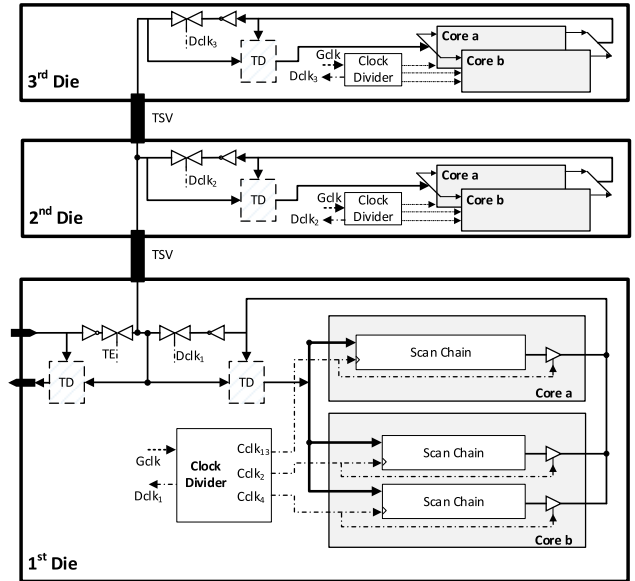

FIGURE 6. SBS-TDM based test access mechanism for the example case of Fig. 1.

operation. The TG also allows turning on and off the transmitters only during the specified intervals to allow time-division multiplexing. The transistor widths were carefully chosen to find the right balance between performance (maximum supported frequency) and acceptable power consumption. This trade-off is discussed further in section V. The transmitter design in Fig. 7(a) is equivalent to a tri-stated inverter whose intermediate nodes between the Pull-up PMOS transistors and Pull-Down NMOS transistors are connected. While this functionality could also be achieved using a tri-state inverter, the transmission-gate based design has an advantage that during the on-state of the transmitter, the effective resistance of the transmission gate is a parallel combination of both the PMOS and NMOS; and therefore, has a lower resistance compared to either NMOS or PMOS. This arrangement reduces delay and improves performance.

The transmitter design must also account for the desired *Vxm* voltage level when the transmitters at either end are in the opposite states. Ignoring the TSV resistance and assuming the pass gate as an ideal switch, the two transmitters' equivalent electrical model when sending opposite signals (10,01) is shown in Fig. 7(b). If R_P and R_N denote the resistance of the PMOS and NMOS transistors of the inverter, respectively, the middle voltage level V_{xm} is given by:

$$V_{xm} = V_{dd}(R_P/(R_P + R_N)) \tag{3}$$

whereas in the triode region:

$$R_p = \frac{1}{\mu_p C_{ox} \frac{W_p}{L} (V_{GS} - V_t)} \tag{4}$$

and,

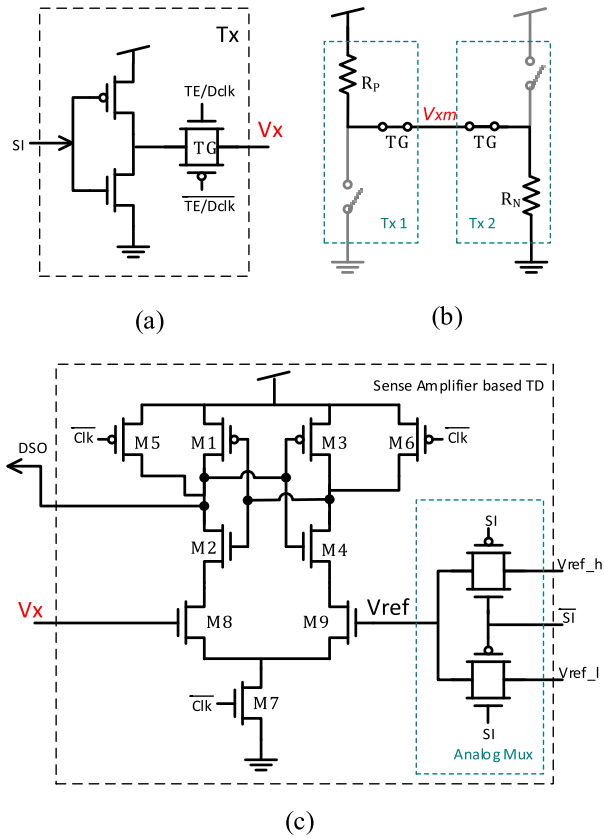$$R_n = \frac{1}{\mu_n C_{ox} \frac{W_n}{L} (V_{GS} - V_t)} \tag{5}$$

FIGURE 7. SBS transceiver implementation (a) Transmitter (b) Equivalent electrical model of the transmitter when sending opposite signals (10,01) (c) Sense-Amplifier based Ternary Decoder (Receiver).

For $Vxm = 1/2$ Vdd, the factors $(V_{GS} - V_t)$ can be assumed to be similar for both PMOS and NMOS, also taking Cox and L to be the same, (3) reduces to:

$$W_p = \frac{\mu_n}{\mu_p} W_n \qquad (6)$$

Therefore, to achieve Vxm = 1/2Vdd, the transistor widths ratio between PMOS and NMOS should be designed so that the on-state current of the low mobility PMOS is similar to higher mobility NMOS. Moreover, the TG transistor sizes are also chosen to be the same for the inverter, ensuring that the TG has a constant on-resistance with the same strength as the inverter.

The Ternary Decoder was designed using a sense-amplifier-based voltage comparator [40], [41] and a pass-gate analog multiplexer, as shown in Fig. 7 (c). The sense amplifier is widely used as a voltage comparator due to its robust operation and power efficiency and is commonly used in high-performance Flash ADCs [42], [43]. The pass-gate analog multiplexer selects the appropriate reference voltage depending on the outgoing signal SI, i.e. the high reference voltage *Vrefh* when SI = 0 and lower reference voltage *Vrefl* when SI = 1. The reference voltage is fed to one sensing input of the sense-amplifier (M9), whereas the other sensing input (M8) receives the ternary coded *Vx* signal. M8 and M9 act like variable resistors with values proportional to
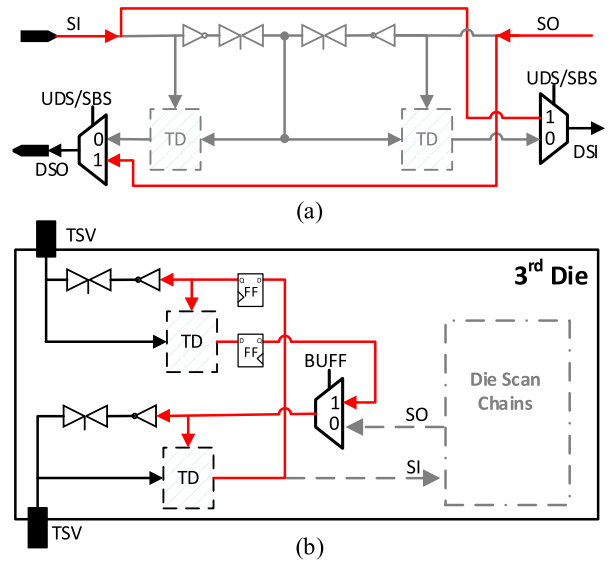

FIGURE 8. (a) Bypass method for pre-bond testing. (b) Using SBS transceivers as buffers to access higher dies.

the respective gate voltage (*Vx* and *Vref*). The transistors M1 through M4 form two cross-coupled inverters. During the positive clock cycle, M5, M6, M2, and M4 turn on, charging the cross-coupled nodes of both inverters to Vdd. During the entire positive clock cycle, the cross-coupled transistors remain in the meta-stable state. During the negative clock half cycle, M7 turns on, providing a discharge path to the cross-coupled inverters; however, the inverters tend to discharge at different rates depending on the on-resistance, and hence the currents through M8 and M9, performing the comparator action through regenerative feedback. The inverting output of the SA amplifier is chosen as the TD's output to reconstruct the original signal, which was inverted by the transmitter designed as an inverter.

B. PRE- AND MID-BOND TESTING
The implementation in Fig. 6 represents the case of post-bond testing in which the dies have been assumed to be already bonded. However, the dies may require testing before bonding, also known as pre-bond testing. As we have considered that the tester communicates using UDS, the pre-bond testing can be undertaken using UDS methods by bypassing the SBS transceivers. This can be achieved by multiplexing the output of the tester side and die side TDs, with the *SO* and *SI* signals, respectively, as shown in Fig. 8(a). The multiplexers may be configured to either select SBS or UDS using a single bit register accessible through JTAG. To minimize power consumption by the SBS transceiver when UDS is selected, the TGs can be turned off, and the TD clock could be disabled by using clock-gating; alternatively, the complete transceiver circuits could be disabled by power-gating. Fig. 8(a) mainly depicts the case for the 1st die; similarly, the SBS transceivers may be bypassed for the other dies.

The mid-bond test instances are a subset of the post bond test problem. However, depending upon the number of dies

	Pseudo-code
1	**Input** (for the current 1-bit global channel)
2	*D* - The number of dies serviced by the channel
3	*S* - the number of scan chain per die
4	*Lc* - length of cores, where c=1toS
5	*x* - vector with scan in bit pattern,
6	*CycReg_die* - Die access sequence for die level clock
7	*CycReg_core* - Core access sequence for core clock
8	**Generate** a 3D array *Scan_chains* with *D* x *S* x *Lc* binary bins
9	**Initialize** *clk=1*, intermediate variables *j=k=y=Input=sel_sc =[ ]*
10	**While** *clk* = true
11	*j= CycReg_core(1)* // currently active core
12	**For** *D* dies,
13	*Input=x(clk)* // current scan-in bit
14	*k= CycReg_die (end)* //currently active die
15	*sel_sc =scan_chains(k, j , 1 to Lc)*
16	*y(clk) = sel_sc(end)*
17	Right-shift *sel_sc* by 1 bit
18	*sel_sc(1)=input*
19	*scan_chains(k, j , 1 to Lc)=sel_sc*
20	*clk++; if clk > length(x)* then **Break** (while)
21	Right-Circular-shift *CycReg_die* by 1 bit
22	**end For**
23	Right-Circular-shift *CycReg_core* by 1 bit
24	**end while**
25	**Output** *y*

FIGURE 9. Pseudo-code for generation of 3D TDM based TAM output for a 1-bit global channel assuming identical dies in the stack.

FIGURE 10. Waveforms of various signals using SBS transceiver design of Fig. 7 in the test setup of Fig. 6 simulated at 1.2 GHz Gclk frequency.

stacked, the clock divider circuit may be multiplexed/ configured accordingly as the case would be in UDS based TDM. However, the addition or removal of the dies may affect the global channel's electrical characteristics, affecting the transmitters' performance and power consumption. The transmitter's performance may be adjusted by using a binary-weighted variable drive strength transmitter [29]. Depending on the requirement, the drive strength may be adjusted by enabling the desired inverters; for instance, a 3-stage transmitter would allow the adjustment of drive strength from 1x to 7x. Similar to the selection of UDS in pre-bond testing, the transmitter strength may be configured using JTAG.

C. TEST SETUP
To test the proposed transceiver, the example 3D stacked die and core structure shown in Fig. 1 was modified to include SBS transceivers as shown in Fig. 6. The TSV was modelled as a lumped RC circuit [6] assuming TSV structure with a length of 20 μm, a diameter of 5 μm, Tox (oxide thickness) of 200nm, and 2×10^{15}/cm^3 doping concentration for the substrate. The resultant RC model has a TSV capacitance of 30fF and resistance of 100 mΩ.

To validate the test structure's output, the typical Capture, Shift, and Update cycle of the scan-chain was ignored, and continuous shifting was performed such that the output is the same as the input. However, it may be noted that unless all the scan-chains are of the same length and operate at the same frequency, the multiplexed output from the scan chains will be an interleaved form of the input. For instance, in the test structure used in this example, *core a* is being serviced using Cclk$_{1,3}$ which is twice the *fmin;* the scan sequence through

this core will appear earlier at the output compared to other scan-chains. To validate the output, the correct/ expected multiplexed output, *SO(expected)*, for the TDM multiplexer can be modeled using the proposed pseudo-code as shown in Fig. 9.

The test setup in Fig. 6 has been limited to 3 dies; but, 3D SICs with any arbitrary number of dies may be tested using SBS based TDM. However, the signal integrity, when traversing multiple dies in a global TSV, must be ensured. In a UDS scheme, buffers can be inserted midway between two consecutive TSVs; in an SBS scheme, digital buffers cannot be used because of the ternary encoding. The authors in [33] discuss the use of accelerators, mid-way latches, and opposite-polarity transition encoding to improve SBS performance in highly lossy global links, and the authors in [44] propose using clamping circuits to address the same. The proposed design does not include any intermediate buffers; there will be an upper limit on the number of dies supported by the given transceiver design for a TDM global channel. The dies higher up the stack may be accessed by using SBS transceivers as buffers. For instance, for the test case in Fig.6, the dies beyond the 3rd die may be accessed using SBS buffers as shown in Fig 8(b). The use of this method has two implications, 1) every SBS buffer instance requires insertion of flip-flops resulting in an additional 1-bit delay in the scan shift cycle, and 2) The overall test schedule would require different sessions to test the buffered segments.

V. RESULTS AND DISCUSSION
Simulations were performed with Cadence Virtuoso using 45nm technology and the standard cells from 45nm Nangate
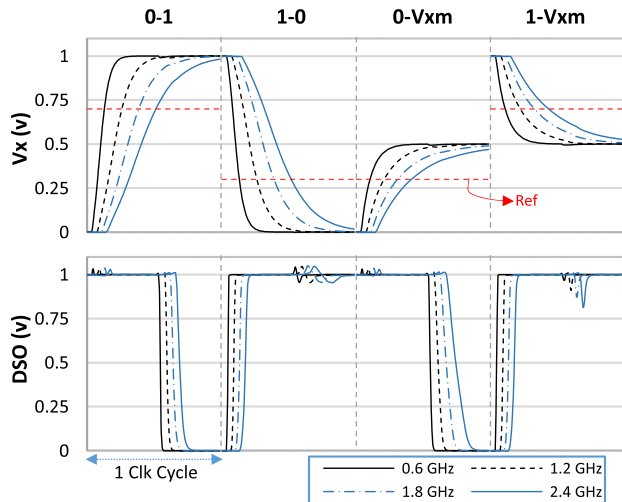
FIGURE 11. Transceiver transient response with varying frequency.

Library [45], using 1v Vdd. The proposed transceiver was designed to achieve an operating frequency of 1.2GHz at the global TSV channel. The transmitter's NMOS transistors were designed with 360nm width, and the PMOS transistors were designed as $1.6 \times$ NMOS width giving the middle voltage level of approximately 0.5Vdd. The Sense-Amplifier was designed using 360nm NMOS width and $1.6 \times$ NMOS width for the PMOS transistors. The lower and upper reference voltages were chosen to be 300mV and 700mV, respectively, for a supply voltage of 1V. From here on, we define the scan-in side transceiver and the scan-out side transceivers as near-end and far-end transceivers, respectively. The transient simulation results for the near-end transceiver at 1.2GHz frequency are shown in Fig. 10. The near-end transmitter sends the scan-in (*SI*) signal, which is demultiplexed to 9 scan chains in 3 dies. Although there are 3 far-end transmitters, only one is active at a time, essentially behaving as a single transmitter, and hence the signal scan-out (*SO*) as seen by the near end transceiver is shown as *SO(expected)* and was computed using the pseudo-code in Fig. 9. The various intermediate signals in the TD are also shown, and the output of TD is denoted as Decoded Scan-Out (*DSO*). The *DSO* signal appears as a unipolar return to zero coded waveform due to the sense-amplifier's nature, which can be directly fed to the scan chains. The signal *SO* in Fig. 10 shows the first scan-flop's reconstructed output and is similar to the *SO(Expected)* signal delayed by 1 cycle.

Fig. 11 compares the transceiver behaviour with varying frequency. The output of the transmitter (*Vx*) and the receiver (*DSO*) are shown for 0.6, 1.2, 1.8, and 2.2 GHz clocks. It may be noted that although there are 3 output states of the Vx signal (0, *Vxm*, and *Vdd*), there are six possible transitions, depending upon the previous state, i.e. rail-trail (0-1,1-0), rail-mid (0-*Vxm*, 1-*Vxm*), and mid-rail (*Vxm*-1, *Vxm*-0). Fig. 11 shows the rail-rail and rail-mid transition, whereas the mid-rail transitions are omitted for clarity as the response is similar to rai-rail. For a given Vx transition, the dashed red markers show the reference

voltage (low or high), which is dependent on SI signal being transmitted. Moreover, for ease of comparison, every interval on the horizontal axis depicts one clock cycle with waveforms for different frequencies accordingly scaled.

From Fig. 11, it is evident that the increasing frequency results in additional gate delay and transient time relative to the clock duration. This results in reduced timing margins and a lesser voltage difference between Vx and Vref at the TD input. While the former affects both the transmitter and receiver and is somewhat mitigated by accounting for timing pessimism, the effect of the latter is rather significant as lesser voltage margins decrease the robustness of the TD, especially in the presence of process variations and cross-coupling. It is interesting to note that although the rail-rail transitions involve a larger voltage swing than the rail-mid swing, they are relatively faster ($\sim$60% compared to the rail-mid transitions). This is because the rail-rail transitions are only possible when both near- and far-end transmitters are being driven in the same direction, which effectively doubles the drive strength. For the same reason, the mid-rail transitions also exhibit similar behaviour, which may even be slightly better due to reduced voltage swing. On the other hand, there is effectively a single transmitter driving Vx for the case of rail-mid transitions, resulting in relatively slower transitions. Consequently, with increasing frequency, the transceiver performance is likely to degrade for the rail-mid transitions first; therefore, the transceiver may be designed considering the rail-mid response as the worst case.

The transceiver operation was verified across all process corners at 1.2GHz. A maximum variation of 40 mV was seen in the mid voltage level *Vxm* across various design corners. It may be noted that the *Vxm* seen by the near and far end transceivers may slightly differ further due to parasitic resistances. The minimum offset voltage (the difference between *Vref* and *Vx*) required to correctly resolve the middle voltage level *Vxm* from *Vrefl* or *Vrefh* (low or high reference voltages) levels was observed to be approximately 25mv. This gives a sufficient margin to account for voltage drops due to parasitics and additional statistical offset due to variability in the sense amplifier

A. POWER CONSUMPTION
The power consumed by the test circuit designed using UDS and SBS based TDM is defined as the sum of average power consumed by the transmitters and receivers when a pseudo-random binary sequence is used as the input. At 1.2 GHz switching frequency, the total power consumption of the complete channel, including 1 x near-end transceiver and 3 x far-end transceivers of the global channel, was 164.5 μW for the SBS based design, which is 22.5% higher as compared to the UDS based scheme (134.2 μW), designed using 4x Buffers as transceivers. The power consumption trend of both designs with increasing frequency of operation is shown in Fig. 12. The power consumption of both methods increases with frequency. However, as the UDS-TDM can be designed using static CMOS, the static power component is
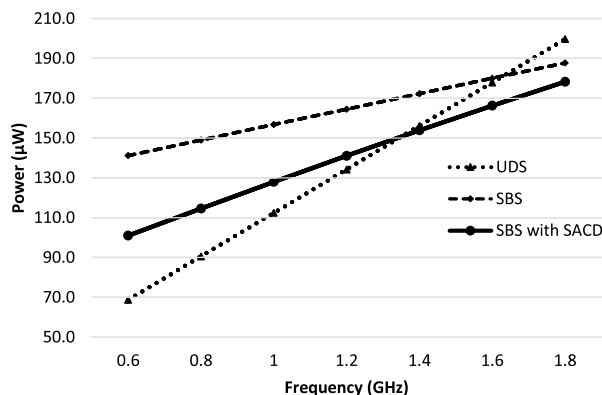
FIGURE 12. Power consumption of a single channel for UDS (Fig. 1) and SBS (Fig. 6) transceiver based TDM schemes.

TABLE 2. Binary-weighted transmitter performance.

Sel bits	Tx Strength	Tx Power (µW)	Max Freq (GHz)
001	x1	52.28	0.67
010	x2	80.00	1.30
011	x3	107.00	1.77
100	x4	135.60	2.06
101	x5	162.80	2.21
110	x6	190.90	2.30
111	x7	218.30	2.46

minimal, and the overall power consumption is dominated by the dynamic power, which increases considerably with the frequency at the rate of 10.9 μW/100MHz. For the SBS based design, the dynamic power consumption is relatively lesser at 3.9 μW/100MHz, which can be attributed to the reduced voltage swing due to 3-level encoding and the relatively smaller transistor sizes. However, the major contributor to the overall power in SBS transceiver is the static power. As the static power consumption remains independent of the frequency, the power consumption of SBS at lower frequencies was observed to be higher than UDS. Nevertheless, due to lower dynamic power consumption, SBS consumes lesser power at higher frequencies as compared to UDS.

The static power consumption can be reduced by limiting the static current when both transmitters transmit the opposite signal, i.e., 10 or 01. To limit static currents and conserve power, designs such as capacitive coupling-based transmitters [37] or MOSR coupled inverters [38] have been proposed. The capacitor-based design significantly improves static power consumption by blocking the steady-state current; however, the capacitor also blocks the noise discharge path making it prone to coupling noise, which may be significant in TDM based TAMs where global channels are required. The MOSR based transmitter limits the static power, but it also reduces the voltage swing and increases transient times/delays, and therefore only finds its use in low-frequency applications. The authors in [41] propose a Sense-Amplifier Completion Detector (SACD) circuit that can turn off one of the transmitters after the TD has compared the inputs. The SACD was incorporated in the test circuit, and the SI side TG was turned off after completion of the sampling by the sense amplifier during every cycle. Fig. 12 compares the power consumption of an SACD-based design which reduces the static power by almost 18%; however, the additional circuit of the SACD adds to the dynamic power, which increases from 3.9 to 6.4 μW/100MHz.

Table 2 presents the transmitter's average power consumption and the maximum frequency when a binary-weighted transmitter is used, as suggested in section IVB. The width for the x1 transmitter was chosen to be 180nm, which is

twice the minimum technology width. The PMOS transistors were sized as 1.6 x NMOS. Similarly, the second and third stage transmitters were sized x2 and x4. The maximum frequency was estimated by measuring the 10-90% rise and fall times between rail to rail and rail to mid-level (Vxm). The reported maximum frequency (*fmax*) is 40% (0.8 × 0.5) of the frequency suggested by the transient response to account for the time required for sampling and sensing at the receiver, i.e. (*fmax* = 0.8 × (0.5/ max[rise-time, fall-time]). Clearly, decreasing the transmitter strength significantly reduces power consumption; however, the weaker transistors also limit the maximum achievable frequency. Therefore, there exists a trade-off between power consumption and maximum frequency, and an optimal transistor strength should be configured.

B. SIGNAL INTEGRITY UNDER CROSS-COUPLING

As the TSVs are a relatively large structure traversing through the entire substrate, cross-coupling between TSVs becomes a significant concern. The authors in [46] presented a lumped RC model of the TSV cross-coupling, which was used to study the SBS transceiver's performance under cross-coupling noise. The RC values were calculated assuming silicon resistivity of 6.89 Ω.cm and a TSV pitch of 10μm. As the test circuit traverses 2 TSVs in the global channel, assuming every TSV is surrounded by 8 neighbouring aggressors (for a 3 × 3 cluster), and each neighbour driven by a PRBS sequence, the eye diagram of the Vx signal at the input of the near end (SI side) TD is shown in Fig 13. For the given transmitter design for 1.2GHz frequency, the transceiver was verified working satisfactorily under cross-coupling in all process corners. Fig. 13 shows that most of the coupling noise diminishes at the negative clock edge (for 50% duty cycle); however, the sampling time may be delayed further by increasing the clock's duty cycle for more robust receiver performance. Moreover, the coupling noise may be reduced using TSV guard rings or using power/ ground TSVs among the neighbouring TSVs [47].

For a given sized transmitter, the eye height and width will decrease with increasing frequency. For correct transceiver operation, the transistor sizing of the transmitter, or in the case of the binary-weighted transmitter, the configuration of the transmitter is to be selected for the appropriate eye-opening at the desired frequency and power. The SA must be sized to account for the affordable offset voltage margin for the chosen reference voltages. The receiver sampling time may

TABLE 3. Comparison with relevant works.

	Signaling Method	Bit pattern	Av. Power @ 1.2GHz	Power Improvement (%)	Max. Freq	Technol- ogy	Channel
This work	SBS/TDM	PRBS	0.165mW	-22.5%	1.2GHz	45nm	-Multiple TSVs
Georgiou et al. [27]	UDS/ TDM	Toggle	0.6mW	NA	3.45GHz	45nm	-Multiple TSVs
Park et al. [36]	SBS	High Data Transition	0.154mW*	+31%	4.55GHz	28nm	-Single TSV
Aung et al. [37]	SBS	PRBS	0.106mW**	-37%**	>3.6GHz	65nm	-Capacitive Coupling

*estimated from reported energy efficiency at 4.55GHz clock
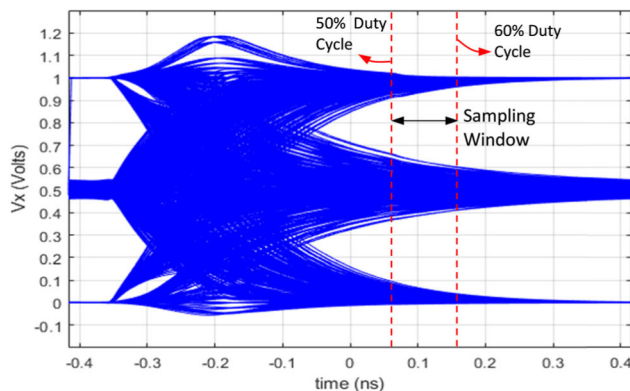**estimated from reported static and dynamic power

FIGURE 13. Eye diagram for the Vx signal at near end receiver side at 1.2GHz under TSV Cross coupling (all process corners).

be adjusted using the clock duty cycle to provide sufficient timing margins.

C. COMPARISON WITH RELEVANT PRIOR WORK

Table 3 compares this work with the other relevant work regarding power consumption improvement over UDS and maximum frequency. The results are compared with relevant previous works in TDM based 3D TAM design [27] and SBS designs for use in 3D SICs [36], [37]. The authors in [27] reported $600\mu W$ average power consumption for a global channel of 3 dies, which is much higher than the SBS transceiver proposed in this paper ($165\mu W$). However, the authors used toggle input, 6x strength transmitters, and intermediate buffers resulting in higher power consumption. The power consumption of SBS and UDS is affected by various factors such as transistor technology, channel characteristics, and the bit patterns used. Therefore, we compare the percentage improvement in power consumption of the relevant SBS design over UDS designed in the same technology reported by the authors for a fair comparison. The SBS design in [37] consumes an estimated 37% more power compared to UDS based scheme, which is slightly more than this work (22.5%). Park *et al.* in [36] reported an SBS transceiver design

that was 33% more power-efficient than UDS transceivers for 2 x TSVs. However, the reported comparison was made at the maximum supported frequency, where it is expected to be more power-efficient, as suggested by the trend in Fig. 12. Another notable factor causing the difference in the power consumption and the maximum supported frequency is that the designs proposed in [36], [37] were focused on a single TSV channel for point to point communication involving 2 x transceivers. On the contrary, a TDM based channel involves multiple dies/ TSVs in the channel involving multiple transceivers (1 near-end and 3 far-end transceivers used in our experiments). These factors increase power consumption and result in lesser frequency in this work than point-to-point communication channels.

Unlike full pin count test methods, which involve designing SBS transceiver at every chip terminal, RPCT based methods use only a subset of chip terminals, and therefore the area overheads are not a significant concern. In general, an SBS-based transceiver occupies an area similar to or slightly higher than the UDS counterpart designed for a similar frequency range [36].

VI. CONCLUSION

A novel SBS-TDM based reduced pin count test strategy was proposed for testing TSV based 3D SICs. Design considerations for the transmitter, receiver, and the control circuitry required for SBS based TDM, and associated trade-offs were presented. The transmitter was designed as a suitably sized inverter followed by a Transmission Gate, and the receiver designed as a Sense Amplifier. The power consumption of the SBS based transceiver is dominated by the static power consumption of the transmitter, which can be minimized using appropriate transistor sizing and control. The limitations of the SBS-based test strategy in terms of the channel's electrical characteristics and possible solutions for the incorporation of SBS into pre-, mid-, and post-bond test instances were discussed. SBS transceiver can be bypassed for pre-bond testing allowing normal UDS communication, whereas adjustable strength SBS transmitters along with SBS buffers

are proposed for mid-bond test insertions. Simulation results using an example test case, in terms of power consumption and performance were presented. The proposed method consumed 22.5% more power while utilizing only half the number of TSVs than the UDS based design. The transceiver performance was verified across all process corners under cross-coupling from neighboring TSVs.

REFERENCES

[1] R. Sharma and K. Choi, *Design of 3D Integrated Circuits and Systems*. Boca Raton, FL, USA: CRC Press, 2014, pp. 157–174.

[2] G. H. Loh, Y. Xie, and B. Black, "Processor design in 3D die-stacking technologies," *IEEE Micro*, vol. 27, no. 3, pp. 31–48, May 2007.

[3] M. B. Healy, K. Athikulwongse, R. Goel, M. M. Hossain, D. H. Kim, Y.-J. Lee, D. L. Lewis, T.-W. Lin, C. Liu, M. Jung, B. Ouellette, M. Pathak, H. Sane, G. Shen, D. H. Woo, X. Zhao, G. H. Loh, H.-H.-S. Lee, and S. K. Lim, "Design and analysis of 3D-MAPS: A many-core 3D processor with stacked memory," in *Proc. IEEE Custom Integr. Circuits Conf.*, Sep. 2010, pp. 1–4.

[4] C. Ababei, P. Maidee, and K. Bazargan, *Exploring Potential Benefits of 3D FPGA Integration*. Berlin, Germany: Springer, 2004, pp. 874–880.

[5] H.-H.-S. Lee and K. Chakrabarty, "Test challenges for 3D integrated circuits," *IEEE Des. Test. Comput.*, vol. 26, no. 5, pp. 26–35, Sep. 2009.

[6] G. Katti, M. Stucchi, K. De Meyer, and W. Dehaene, "Electrical modeling and characterization of through silicon via for three-dimensional ICs," *IEEE Trans. Electron Devices*, vol. 57, no. 1, pp. 256–262, Jan. 2010.

[7] H. Vranken, T. Waayers, H. Fleury, and D. Lelouvier, "Enhanced reduced pin-count test for full-scan design," *J. Electron. Test. Theory Appl.*, vol. 18, no. 2, pp. 129–143, 2002.

[8] A. C. Evans, "Applications of semiconductor test economics, and multisite testing to lower cost of test," in *Proc. Int. Test Conf.*, 2003, pp. 113–123.

[9] A. H. Baba and K. S. Kim, "Framework for massively parallel testing at wafer and package test," in *Proc. IEEE Int. Conf. Comput. Des. VLSI Comput. Process.*, Oct. 2009, pp. 328–334.

[10] M. L. Bushnel and V. D. Agrawal, *Essentials of Electronic Testing for Digital, Memory and Mixed-Signal VLSI Circuits*. Norwell, MA, USA: Kluwer, 2002.

[11] *IEEE Standard for Test Access Port and Boundary-Scan Architecture*, IEEE Standard 1149.1-2013 (Revision IEEE Std 1149.1-2001), 2013, pp. 1–444.

[12] *IEEE Standard Testability Method for Embedded Core-Based Integrated Circuits*, IEEE Standard 1500-2005, 2005, pp. 1–136.

[13] *IEEE Standard for Test Access Architecture for Three-Dimensional Stacked Integrated Circuits*, IEEE Standard 1838-2019, 2020, pp. 1–73.

[14] N. A. Touba, "Survey of test vector compression techniques," *IEEE Des. Test. Comput.*, vol. 23, no. 4, pp. 294–303, Apr. 2006.

[15] V. Iyengar, K. Chakrabarty, and E. J. Marinissen, "Test wrapper and test access mechanism co-optimization for system-on-chip," *J. Electron. Test. Theory Appl.*, vol. 18, pp. 213–230, Apr. 2002.

[16] X. Wu, Y. Chen, K. Chakrabarty, and Y. Xie, "Test-access mechanism optimization for core-based three-dimensional SOCs," in *Proc. IEEE Int. Conf. Comput. Design*, Oct. 2008, pp. 212–218.

[17] E. J. Marinissen, "Challenges and emerging solutions in testing TSV-based 2 1 over 2D- and 3D-stacked ICs," in *Proc. Design, Automat. Test Eur. Conf. Exhib. (DATE)*, Mar. 2012, pp. 1277–1282.

[18] *IEEE Standard for Access and Control of Instrumentation Embedded Within a Semiconductor Device—1687*, IEEE Standard 1687-2014, 2014, pp. 1–283.

[19] M. A. Ansari, J. Jung, D. Kim, and S. Park, "Time-multiplexed 1687-network for test cost reduction," *IEEE Trans. Comput.-Aided Design Integr. Circuits Syst.*, vol. 37, no. 8, pp. 1681–1691, Aug. 2018.

[20] A. Sehgal, V. Iyengar, and K. Chakrabarty, "SOC test planning using virtual test access architectures," *IEEE Trans. Very Large Scale Integr. (VLSI) Syst.*, vol. 12, no. 12, pp. 1263–1276, Dec. 2004.

[21] A. Sanghani, B. Yang, K. Natarajan, and C. Liu, "Design and implementation of a time-division multiplexing scan architecture using serializer and deserializer in GPU chips," in *Proc. 29th VLSI Test Symp.*, May 2011, pp. 219–224.

[22] M. S. Kawoosa, R. K. Mittal, M. Jalasuthram, and R. A. Parekhji, "Towards single pin scan for extremely low pin count test," in *Proc. 31st Int. Conf. VLSI Design 17th Int. Conf. Embedded Syst. (VLSID)*, Jan. 2018, pp. 97–102.

[23] B. Li and V. D. Agrawal, "Applications of mixed-signal technology in digital testing," *J. Electron. Test.*, vol. 32, no. 2, pp. 209–225, Apr. 2016.

[24] B. Noia, K. Chakrabarty, S. K. Goel, E. J. Marinissen, and J. Verbree, "Test-architecture optimization and test scheduling for TSV-based 3-D stacked ICs," *IEEE Trans. Comput.-Aided Design Integr. Circuits Syst.*, vol. 30, no. 11, pp. 1705–1718, Nov. 2011.

[25] X. Wu, P. Falkenstern, K. Chakrabarty, and Y. Xie, "Scan-chain design and optimization for three-dimensional integrated circuits," *ACM J. Emerg. Technol. Comput. Syst.*, vol. 5, no. 2, pp. 1–26, Jul. 2009.

[26] M. A. Ansari, J. Jung, D. Kim, and S. Park, "Time-multiplexed test access architecture for stacked integrated circuits," *IEICE Electron. Exp.*, vol. 13, no. 14, 2016, Art. no. 20160314.

[27] P. Georgiou, F. Vartziotis, X. Kavousianos, and K. Chakrabarty, "Testing 3D-SoCs using 2-D time-division multiplexing," *IEEE Trans. Comput.-Aided Design Integr. Circuits Syst.*, vol. 37, no. 12, pp. 3177–3185, Dec. 2018.

[28] B. G. West, "Simultaneous bidirectional test data flow for a low-cost wafer test strategy," in *Proc. Int. Test Conf. (ITC)*, vol. 1, Jan. 2003, pp. 947–951.

[29] R. Mooney, C. Dike, and S. Borkar, "A 900 Mb/s bidirectional signaling scheme," *IEEE J. Solid-State Circuits*, vol. 30, no. 12, pp. 1538–1543, Dec. 1995.

[30] H.-Y. Huang and R.-I. Pu, "Differential bidirectional transceiver for on-chip long wires," *Microelectron. J.*, vol. 42, no. 11, pp. 1208–1215, Nov. 2011.

[31] Y. Tomita, H. Tamura, M. Kibune, J. Ogawa, K. Gotoh, and T. Kuroda, "A 20-Gb/s simultaneous bidirectional transceiver using a resistor-transconductor hybrid in 0.11-μ CMOS," *IEEE J. Solid-State Circuits*, vol. 42, no. 3, pp. 627–636, Mar. 2007.

[32] J.-Y. Sim, Y.-S. Sohn, S.-C. Heo, H.-J. Park, and S.-I. Cho, "A 1-Gb/s bidirectional I/O buffer using the current-mode scheme," *IEEE J. Solid-State Circuits*, vol. 34, no. 4, pp. 529–535, Apr. 1999.

[33] C. J. Akl and M. A. Bayoumi, "Wiring-area efficient simultaneous bidirectional point-to-point link for inter-block on-chip signaling," in *Proc. IEEE Int. Freq. Control Symp. Expo.*, Jan. 2008, pp. 193–200.

[34] M.-K. Jeon and C. Yoo, "A single-ended simultaneous bidirectional transceiver in 65-nm CMOS technology," *J. Semicond. Technol. Sci.*, vol. 16, no. 6, pp. 817–824, Dec. 2016.

[35] P. V. S. Rao and P. Mandal, "Current-mode full-duplex (CMFD) signaling for high-speed chip-to-chip interconnect," *Microelectron. J.*, vol. 42, no. 7, pp. 957–965, Jul. 2011.

[36] S. Park, A. Wang, U. Ko, L.-S. Peh, and A. P. Chandrakasan, "Enabling simultaneously bi-directional TSV signaling for energy and area efficient 3D-ICs," in *Proc. Design, Automat. Test Eur. Conf. Exhib. (DATE)*, 2016, pp. 163–168.

[37] M. T. L. Aung, E. Lim, T. Yoshikawa, and T. T.-H. Kim, "Design of simultaneous bi-directional transceivers utilizing capacitive coupling for 3DICs in face-to-face configuration," *IEEE J. Emerg. Sel. Topics Circuits Syst.*, vol. 2, no. 2, pp. 257–265, Jun. 2012.

[38] I. A. Soomro, M. Samie, and I. K. Jennions, "Test time reduction of 3-D stacked ICs using ternary coded simultaneous bidirectional signaling in parallel test ports," *IEEE Trans. Comput.-Aided Design Integr. Circuits Syst.*, vol. 39, no. 12, pp. 5225–5237, Dec. 2020.

[39] N. Wary and P. Mandal, "Current-mode simultaneous bidirectional transceiver for on-chip global interconnects," in *Proc. 6th Asia Symp. Qual. Electron. Design (ASQED)*, Aug. 2015, pp. 19–24.

[40] T. Na, S.-H. Woo, J. Kim, H. Jeong, and S.-O. Jung, "Comparative study of various latch-type sense amplifiers," *IEEE Trans. Very Large Scale Integr. (VLSI) Syst.*, vol. 22, no. 2, pp. 425–429, Feb. 2014.

[41] T. Kobayashi, K. Nogami, T. Shirotori, and Y. Fujimoto, "A current-controlled latch sense amplifier and a static power-saving input buffer for low-power architecture," *IEEE J. Solid-State Circuits*, vol. 28, no. 4, pp. 523–527, Apr. 1993.

[42] Y. Chen, P. I. Mak, J. Yang, R. Yue, and Y. Wang, "Comparator with built-in reference voltage generation and split-ROM encoder for a high-speed flash ADC," in *Proc. Int. Symp. Signals, Circuits Syst. (ISSCS)*, 2015, pp. 2–5.

[43] J. Yang, Y. Chen, H. Qian, Y. Wang, and R. Yue, "A 3.65 mW 5 bit 2GS/s flash ADC with built-in reference voltage in 65 nm CMOS process," in *Proc. IEEE 11th Int. Conf. Solid-State Integr. Circuit Technol. (ICSICT)*, Oct. 2012, pp. 5–7.

[44] M. T. L. Aung, E. Lim, T. Yoshikawa, and T. T.-H. Kim, "A 3-Gb/s/ch simultaneous bidirectional capacitive coupling transceiver for 3DICs," *IEEE Trans. Circuits Syst. II, Exp. Briefs*, vol. 61, no. 9, pp. 706–710, Sep. 2014.

[45] *Nangate 45 nm FreePDK Library*. Accessed: Oct. 3, 2019. [Online]. Available: https://si2.org/open-cell-library/

[46] T. Song, C. Liu, Y. Peng, and S. K. Lim, "Full-chip signal integrity analysis and optimization of 3-D ICs," *IEEE Trans. Very Large Scale Integr. (VLSI) Syst.*, vol. 24, no. 5, pp. 1636–1648, May 2016.

[47] Y. Peng, T. Song, D. Petranovic, and S. K. Lim, "Silicon effect-aware full-chip extraction and mitigation of TSV-to-TSV coupling," *IEEE Trans. Comput.-Aided Design Integr. Circuits Syst.*, vol. 33, no. 12, pp. 1900–1913, Dec. 2014.

MOHAMMAD SAMIE received the B.Sc. degree in electronics from the Islamic Azad University of Saveh, Iran, in 1997, the M.Sc. degree in electronics from Shiraz University, Shiraz, Iran, in 2002, and the Ph.D. degree in advanced electronics from the University of the West of England, Bristol, U.K., in 2012.

He is currently working as a Lecturer with the School of Aerospace, Transport and Manufacturing (SATM), Cranfield University, U.K. He is also leading Seretonix, the Secure and Reliable Electronic Systems Group, Cranfield University, with a focus on resilience and security of electronics. He has accumulated a wide and varied experience in field programmable gate arrays (FPGAs) and ASIC design, simulation, verification, and implementation, Toumaz in Didcot, U.K. He was involved with two EPSRC-funded projects NFF and SABRE, where he was responsible for creating most of the detailed designs and implementations. He has published 36 international journals, conference papers, and book chapters, with two awarded as best articles, on bio-inspired electronics.

IFTIKHAR A. SOOMRO received the B.E. degree in electronics engineering and the M.S. degree in electrical engineering (control systems) from the National University of Sciences and Technology (NUST), Karachi, Pakistan, in 2007 and 2017, respectively. He is currently pursuing the Ph.D. degree in manufacturing engineering (electronics) with the Integrated Vehicle Health Management (IVHM) Centre, School of Aerospace, Transport, and Manufacturing (SATM), Cranfield University, U.K.

His research interests include reliability, mixed-signal sensor design, testability, and prognostics in electronic circuits and systems.

Mr. Soomro was a recipient of the President's, Rector's, and CNS Gold medals for his B.E. degree, and the President's Gold Medal for his M.S. degree.

IAN K. JENNIONS received the degree in mechanical engineering and the Ph.D. degree in CFD from Imperial College London, London.

He has worked for Rolls-Royce (twice), General Electric, and Alstom in a number of technical roles, gaining experience in aerodynamics, heat transfer, fluid systems, mechanical design, combustion, services, and IVHM. In July 2008, he moved to Cranfield University, as a Professor, and the Director of the IVHM Centre which is funded by a number of industrial companies, including Boeing, BAE Systems, Thales, Meggitt, MOD, DRS, Alstom Transport, and Novartis. He has led the development and growth of the IVHM Centre, in research and education, since its inception. His career spans some 40 years, working mostly for a variety of gas turbine companies. He has coauthored the book *No Fault Found—The Search for the Root Cause*. He is the Editor of five SAE books on IVHM and the recent *The World of Civil Aerospace*. He is a Fellow of IMechE, RAeS, ASME, and PHM, a Contributing Member of the HM-1 IVHM Committee, the Director of the PHM Society, and a Chartered Engineer. He is the Chair of the SAE IVHM Steering Group. He represents the Editorial Board of the *International Journal of Condition Monitoring*.

• • •